Phys Chem Minerals (2008) 35:77–93
DOI 10.1007/s00269-007-0200-8

ORIGINAL PAPER

Advanced analyses of ^{57}Fe Mössbauer data of alumino-silicate glasses

S. Rossano · H. Behrens · M. Wilke

Received: 26 June 2007 / Accepted: 19 October 2007 / Published online: 20 November 2007

Abstract ^{57}Fe Mössbauer spectra of iron bearing alumino-silicate glasses are analysed by two complementary methods (SID and x-VBF) especially adapted for the analysis of disordered systems by taking into account distributions of hyperfine Mössbauer parameters. Qualitative and quantitative information about the oxidation state of iron are obtained as well as information about the distribution of local environments of iron. The possibility to separate the signal of ferric iron from that of ferrous iron allows to derive precise redox ratio in favourable cases but also to analyse more sharply the different contributions to Mössbauer spectra. Using two different glass series (feldspar composition, haplo-tonalitic composition), the characteristics of the two methods are described and employed to study the effect of composition, water incorporation and oxidation state on the glass structure. Optical absorption spectroscopy is used to support the interpretation of the Mössbauer spectra in case of the feldspar glasses.

S. Rossano (✉)
Université Paris-Est, Lab. des Géomatériaux et Géologie de l'Ingénieur (G2I), EA 4119, 5 Bd Descartes, 77454 Marne la Vallée cedex 2, France
e-mail: stephanie.rossano@univ-mlv.fr

H. Behrens
Institut für Mineralogie, Universität Hannover, Callinstraße 3, 30167 Hannover, Germany

M. Wilke
Institut für Geowissenchaften, Mineralogie-Petrologie, Universität Potsdam, Karl-Liebknecht Str 24, 14476 Golm, Germany

Present Address:
M. Wilke
GeoForschungZentrum Potsdam, Telegrafenberg, 14473 Potsdam, Germany

Keywords Mössbauer · Glass · Iron · Site distribution · Oxidation state

Introduction

Iron is a major component of natural and technological silicate glasses and melts if one considers its abundance (up to 15 wt% in magmatic rocks) but also its influence on glass/melt properties (see Mysen and Richet 2005 for a review). Its particularity to be present in various oxidation states (metallic, ferrous or ferric) makes it a sensitive probe of the redox conditions of melt/glass and rock formation provided that the redox ratio is precisely determined and the relationship to other intensive and extensive parameters is known. From a technological point of view, the ability of iron to change its oxidation state is crucial for the structural evolution of glasses under irradiation (Boizot et al. 2005) or the absorption of light in the IR or UV range (Lefrère 2002; Uchino et al. 2000). Because structure and physico-chemical properties are intimately related, the structural environment of iron in glasses and melts has to be investigated to better understand the role of iron in natural and technological systems.

Mössbauer spectroscopy is a powerful tool to obtain quantitative information on both the structural environment and oxidation state of iron in silicate glasses and melts among various spectroscopic methods such as X-ray absorption spectroscopy (Calas and Petiau 1983; Hannoyer et al. 1992; Mosbah et al. 1999; Rossano et al. 2000a; b; Wilke et al. 2001; Galoisy et al. 2001; Bonnin-Mosbah et al. 2001, 2002; Giuli et al. 2003, 2005; Berry et al. 2003; Antoni et al. 2004; Farges et al. 2004; Quartieri et al. 2005; Botcharnikov et al. 2005; Jackson et al. 2005; Wilke et al. 2005, 2006; Metrich et al. 2006; Magnien et al.

2006), optical absorption spectroscopy (Hannoyer et al. 1992; Leister and Ehrt 1999; Ehrt et al. 2001; Lefrère 2002), and optical magnetic circular dichroism (Jackson et al. 2005). Individual iron species without magnetic interaction typically display a doublet in Mössbauer spectra. The isomer shift (IS) and quadrupole splitting (QS) of the Mössbauer signal provides information on the oxidation state, coordination number and site geometry of iron species. For more information on Mössbauer spectroscopy and its application to Earth sciences see (Amthauer et al. 2004; Mc Cammon 2004) and references therein.

The conventional method for analysing Mössbauer spectra consists of fitting experimental spectra with Lorentzian doublets associated to the different iron environments occurring in the sample. The redox ratio (Fe^{3+}/Fe^{2+}) is classically derived by evaluating the ratio of the area of the ferric iron contribution to the ferrous iron one. In the case of crystals, the number of iron sites is usually small and site geometries are usually well defined so that the number of doublets to be used can be physically constrained providing an unambiguous way for determining Mössbauer parameters. In the case of glasses, the iron environment (either ferric or ferrous) can differ from one site to the other leading to a distribution of site geometries and thus of both IS and QS values (Levitz et al. 1980; Alberto et al. 1996; Rossano et al. 1999; Mysen 2006). This distribution of sites actually explains the broad and asymmetric shape of Mössbauer spectra measured on glasses. Therefore, the decomposition of Mössbauer spectra into a set of distinct doublets becomes arbitrary for glasses because the number of doublets is unknown and depends probably strongly on glass composition. For all these reasons, nowadays methods are preferred for analyzing Mössbauer spectra using distributions of hyperfine parameters, either distributions of QS only (Dunlap 1997; Karabulut et al. 2002; Partzsch et al. 2004; Botcharnikov et al. 2005; Gunnlaugsson 2006) or distributions of both Mössbauer parameters IS and QS simultaneously (Levitz et al. 1980; Alberto et al. 1996; Rossano et al. 1999; Wilke et al. 2002; Mysen 2006). In the case of samples showing a magnetic behaviour, magnetic field distributions can also be extracted (Nemtsova 2006). Similar advanced techniques were applied for magnetically ordered materials (Lagarec and Rancourt 1997), paramagnetic state materials or minerals presenting distributions of local distortion or local chemical environments (Rancourt et al. 1994a, b, 1996). The full interpretation of the shape of the obtained distributions necessitates ab initio electronic structure calculations to relate the local environment to the hyperfine parameters (Evans et al. 2005). This is however, not yet possible for glasses due to the difficulty to calculate glass electronic structure.

This paper aims to illustrate the amount and the quality of information that can be extracted from spectra measured on glasses synthesized under variable conditions (dry or hydrous, variable oxygen fugacity and quench rate). Experimental spectra were analysed using two different methods that give access to the distribution of hyperfine parameters (IS and QS in our case). These two methods are described in details elsewhere (Rossano et al. 1999; Alberto et al. 1996) and only their main characteristics are summarized in this paper. The first method, so called shape independent distribution (SID) method is designed to extract the probability density distribution (PDD) of a set of elemental doublets of Lorentzian lines described by IS and QS Mössbauer parameters (Rossano et al. 1999). In practical, a grid of (IS,QS) values is considered to fit the experimental spectrum and the relative weight of each Mössbauer doublet is determined using a quadratic minimization procedure (Levitz et al. 1980; Balan et al. 1999; Rossano et al. 1999). This mathematical procedure allows the determination of the true minimum of the system due to the positive semi-definite character of the Hessian matrix of the quadratic objective function ensuring the unicity of the obtained solution. A great advantage of the SID method is that no assumption is made on the iron speciation prior to analysis. The obtained distribution is the envelope of all Mössbauer doublet probabilities.

The second method, so called extended Voigt-Based Fitting (x-VBF) method, is based on the decomposition of the experimental spectrum using Gaussian distributions of Lorentzian doublets (Alberto et al. 1996; Rossano et al. 1999). In contrary to the SID method, assumptions about the number of distributions are needed. The envelope of all distributions can be compared to the one obtained by the SID method in order to validate the mathematical fit. The analysis of the individual distributions in x-VBF provides information about the Mössbauer parameters of the various iron species contributing to the Mössbauer signal while the SID method provides only average apparent parameters (position of the maxima). The comparison of probability distributions provides qualitative information about the structural iron environment in these compounds. Quantitative information such as redox ratio of iron or Mössbauer parameter of ferrous and ferric ions can be extracted in advantageous cases as well as the widths of ferrous and ferric iron distributions.

Samples and analytical methods

Two sets of samples have been analysed in this study. The first one consists of synthetic glasses with feldspar base compositions albite ($NaAlSi_3O_8$, Ab), orthoclase ($KAlSi_3O_8$, Or) and anorthite ($CaAl_2Si_2O_8$, An) containing about 0.5 wt% of iron oxide (Fe_2O_3). The samples are labelled as Ab06, Or06 and An06, respectively. These

simple compositions enable to analyse the effects of the network modifiers Na^+, K^+ and Ca^{2+} on the iron incorporation in polymerized alumino-silicate glasses. Low total iron concentration were chosen in order to be able to measure additionally optical absorption spectra dominated by crystal field transitions and to minimize superimposition of strong bonds due to Fe^{2+}–Fe^{3+} charge transfer. Dry glasses were synthesized in air at 1,600°C during 3 days starting from a mixture of glass powder and Fe_2O_3. The iron oxide was obtained by 30 min oxidation of pure ^{57}Fe foil at 1,000°C in air. One hydrous glass (Or06hyd1) was synthesized in a platinum capsule in an internally heated gas pressure vessel at 1,000°C, 2 kbar for 24 h under intrinsic f_{H2} conditions (Berndt et al. 2002) starting from anhydrous Or06 glass powder to which 5 wt% water was added. The dry Ab06 and Or06 glasses contain few bubbles while Or06hyd1 and An06 are bubble-free. Composition and chemical homogeneity was verified by electron microprobe analyses (Table 1).

^{57}Fe Mössbauer absorption spectra of sample set 1 were all recorded at room temperature with a Wissel conventional constant acceleration Mössbauer device with ^{57}Co (in Rh) source in the range ±4 mm/s in 1,024 channels using the 14.4 keV radiation at the Wissenschaftliches Zentrum für Materialwissenschaften und Institut für Mineralogie, Marburg (Germany). The isomer shifts were recorded relative to α-Fe metal. The absorber sample thickness was optimized following the published procedure of (Rancourt et al. 1993). Typically 150 mg of sample were used for a square surface of 1 cm^2. Additionally, we measured optical absorption spectra of thick sections (thickness of 2.00 ± 0.02 mm, measured with a micrometer) of the nominally dry glasses to get further insights to the incorporation mechanisms of iron in the glasses. Samples were mounted on a hole aperture of 2 mm in diameter. Spectra were recorded in the UV/VIS (10,000–35,000 cm^{-1}) using a spectrometer SPECORD S10 and in the near-infrared (2,000–11,000 cm^{-1}) using an FTIR spectrometer Bruker IFS88.

Table 1 Microprobe analysis (oxide wt%) of dry and hydrous samples in the feldspar system

	Ab06	Or06	Or06hyd1	An06
Na_2O	10.20(50)	0.08(05)	0.07(03)	0.19(04)
K_2O	0.02(01)	14.77(29)	13.67(27)	0.03(02)
CaO	0.02(02)	0.01(01)	0.01(01)	20.50(17)
Al_2O_3	19.65(22)	18.51(11)	17.23(20)	36.13(19)
Fe_2O_3	0.56(09)	0.59(06)	0.49(07)	0.62(09)
SiO_2	69.21(30)	65.64(48)	62.10(60)	42.46(28)
Total	99.83(54)	99.59(31)	93.50(31)	100.00(61)
H_2O	0.017	0.016	4.99	0.012

Oxide components were measured with an electron microprobe CAMECA CAMEBAX. Measurement conditions were: acceleration voltage of 15 kV, beam current of 5 nA, beam defocused to 20 μm, 5 s on peak for Na and K, 10 s on peak for other elements. H_2O contents of nominally dry glasses were determined by IR spectroscopy by measuring the height of the 3,550 cm^{-1} band using a molar absorption coefficient of 67 l/mol cm (Stolper 1982). The H_2O content of Or06hyd1 was measured using Karl–Fisher titration

The second set of samples is an extension of the composition towards more complex natural melt composition. A series of hydrous glasses in the tonalite system SiO_2(Qz)–$NaAlSi_3O_8$(Ab)–$CaAl_2Si_2O_8$(An)–H_2O doped with 1.5 wt% Fe_2O_3 (enriched in ^{57}Fe). The anhydrous glass was synthesized from oxides and carbonates at 1,600°C with a duration of synthesis of 2 × 2 days. 200–400 mg of the resulting anhydrous glass were enclosed in $Ag_{75}Pd_{25}$ capsules together with 12 wt.% water. The glass synthesis was done in two steps. First, all capsules were annealed at 1,000°C and 500 MPa for 24 h at intrinsic oxygen fugacity to homogenize the samples in water content. After checking for mass loss by weighing, the samples were annealed in a second step under controlled oxygen fugacity. These syntheses were performed at 850 and 950°C and 500 MPa for 24 h. More details about the synthesis conditions and room temperature Mössbauer spectra of the samples are published in Wilke et al. (2002). In that previous work, samples were analysed using the SID method and classic fitting of Lorentzian doublets. Here we employed the x-VBF method to further evaluate Mössbauer parameter distributions. To facilitate the comparison between the results obtained by the two methods some of the 3D and 2D plots already published in Wilke et al. (2002) are included in this work. Probability distributions are plotted on 3D and 2D graphs. The 3D graph plots the probability for a specific Mössbauer doublet to contribute to the experimental spectrum as a function of IS and QS. The 2D graph is obtained by projecting the 3D distributions onto the (IS,QS) plane. One of the most striking features of these 2D and 3D representations is that the (IS,QS) range for ferric iron is different from the (IS,QS) range for ferrous iron. Mössbauer parameters for Fe^{3+} are in the IS range of (0–0.6 mm/s) and QS range of (0-1.5 mm/s) while for Fe^{2+}, the IS range is (0.6–2 mm/s) and the QS range is (0.8–2 mm/s). The SID analyses of the glasses were performed with a grid of 30 × 30 points with isomer shift varying in the range (0–2 mm/s) and quadrupole splitting varying in the range (0–3.5 mm/s). In both SID and x-VBF analytical methods, the Lorentzian line width of each elemental doublet was fixed equal to iron signal width at room temperature (0.369 mm/s in this study). Coefficients for the smoothing of the PDD were chosen equal to 1.7 for all samples in the SID method (see Levitz et al. 1980; Balan et al. 1999 for more details about these coefficients).

Results and discussion

Network modifier effect

Mössbauer spectra of the Ab06, An06 and Or06 glasses are presented on Fig. 1. These spectra are mainly composed of a broad and asymmetric doublet due to the Mössbauer effect of ferrous iron. The high asymmetry of the doublet indicates the presence of a broad distribution of the Fe^{2+} environment. Superimposed on the ferrous iron doublet, a feature, peaking around 1 mm/s, is clearly visible on the Ab06 spectrum. It is due to the high velocity branch of the ferric iron Mössbauer signal. Although not clearly resolved for Or06, this feature modifies the shape of the region around 1 mm/s, as well. By contrast, the Mössbauer spectrum of the An06 sample is typical for a quasi 100% reduced glass [see for comparison tektite spectra (Rossano et al. 1999)]. The Ab06 glass appears to be the most oxidized of the three compositions as the Fe^{3+} feature around 1 mm/s is clearly visible. The Or06 sample oxidation state is probably intermediate between the two other compositions.

This trend in the oxidation state is corroborated by optical absorption spectroscopy. Optical absorption spectra in the near infra-red (NIR) and visible range of the three samples AnO6, OrO6 and AbO6 are displayed on Fig. 2. The absorption band for ferrous iron, located in the NIR region (between 4,500 and 20,000 cm^{-1}) has the highest intensity for the AnO6 sample. In contrast, the absorption band for ferric iron, which appears near the UV edge, is only visible for the Ab06 sample. In good agreement with Mössbauer results, the OrO6 sample is intermediate between AnO6 and AbO6. However, it has to be emphasized that the absorption coefficients of iron ions may be different from one composition to the others and, hence, peak areas do not directly represent species concentrations. The Fe^{3+} transitions are both spin-forbidden and Laporte-forbidden and small variations in local geometry may have a strong effect on the absorptivity.

The distributions obtained by the SID method are presented on Fig. 3. We can immediately notice a difference between the An06 sample on the one hand and the Ab06 and Or06 samples on the other hand. The distribution obtained for the An06 sample is similar to the few distributions already published for the $CaO–SiO_2–Fe–O$ glass system (Alberto et al. 1996) and for tektite glasses (Rossano et al. 1999), i.e. almost completely reduced glasses. It is composed of a strong maximum at IS = 1.1 and QS = 2 mm/s that has been previously attributed to fivefold coordinated ferrous iron (Rossano et al. 1999). At lower IS and QS values, a second maximum (IS = 0.6 and QS = 1 mm/s) is attributed to fourfold coordinated ferrous iron by comparison with crystalline references (Burns 1994). Finally an additional small feature is visible in the 3D plot at IS around 0.25 mm/s and QS around 0.5 mm/s. This feature which is attributed to ferric iron in a tetrahedral site (Burns 1994) is not visible in the contour plots, because of its weak relative intensity as compared to the two other components.

By contrast, the distributions for Ab06 and Or06 show a complex very broad feature covering continuously the ferric iron region and the ferrous iron one. If examined in more detail, the distribution appears to be more structured for Ab06 as compared to Or06. Three distinct maxima are

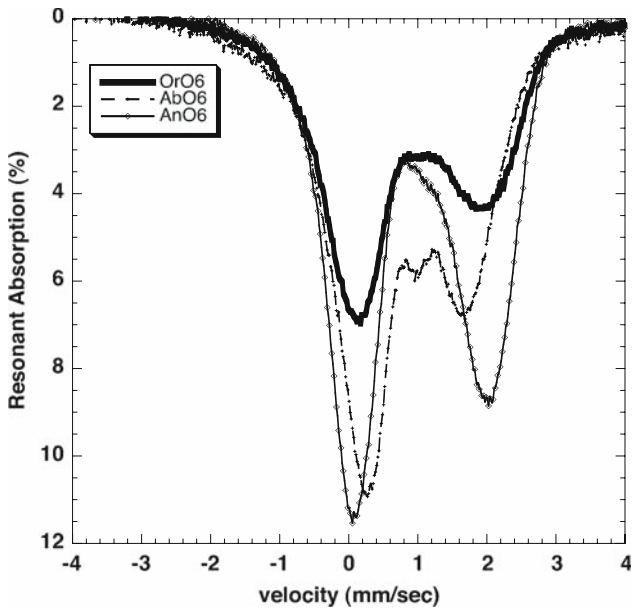

Fig. 1 Mössbauer spectra of AbO6, OrO6 and AnO6 glasses

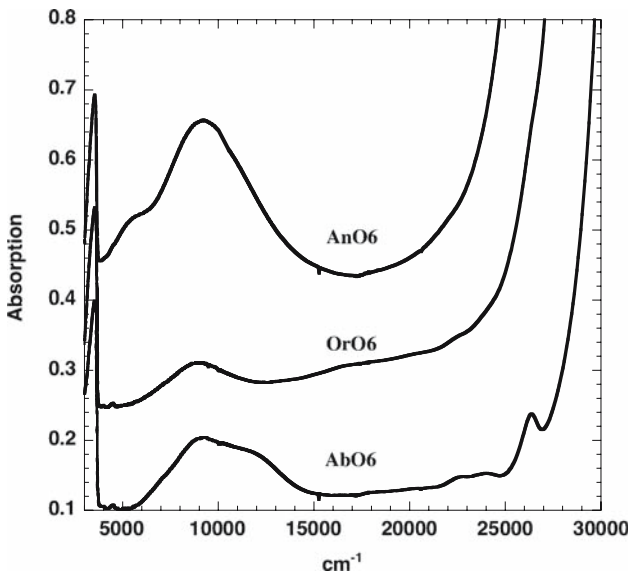

Fig. 2 NIR and visible optical absorption spectra of An06, Or06 and Ab06 samples

visible that can be attributed to two ferrous iron and one ferric iron environments. Considering the broadness of these distributions no attempt was made to analyse in detail the coordination of ferrous iron. All coordination numbers (4, 5 or 6) are probably present in these glasses in a continuous distribution of environments as was shown for ferrous iron in $CaFeSi_2O_6$ by X-ray absorption spectroscopy and molecular dynamics simulation (Rossano et al. 2000a).

This interpretation is clearly supported by the shape of the ferrous iron absorption band in the NIR region (Fig. 2), which varies strongly from one glass to the other. The ferrous iron absorption band of An06 sample shows two maxima located at 5,330 and 9,130 cm^{-1} while Ab06 sample displays two maxima located at 9,100 and 11,730 cm^{-1}. In contrast, the ferrous iron absorption band of Or06 sample shows one maximum only located at 8,980 cm^{-1}. Although still debated (see Lefrère 2002 and references therein) these variations can be attributed to variations in coordination (4 + 5 + 6) and/or distortion effects. Differences in the ferric iron environment cannot be distinguished due to the poor resolution and low intensity of the ferric iron absorption bands near 25,000 cm^{-1}. Only in the case of the Ab06 sample, Fe^{3+} bands are clearly resolved with shapes similar to those observed for feldspar minerals (e.g. Hofmeister and Rossman 1984). The feature located at low IS and QS (i.e. the ferric iron signal) is more intensive for Ab06 and Or06 glasses than for An06 glass suggesting again the higher Fe^{3+}/Fe_{tot} ratio of these two samples. Due to the very broad shape of the Mössbauer spectra, the x-VBF method is not adapted to fit the Or06 and Ab06 spectra. Indeed, a very high number of distributions will have to be considered leading to a mathematical fit with no physical meaning. A fit of the An06 spectrum could be performed but does not help understanding the differences observed as the comparison with the two other compositions is missing.

Glasses of albite, orthoclase and anorthite compositions are characterized by a completely polymerized network. The electrical charge due to AlO_4^- groups is balanced by alkali (K^+ or Na^+) or alkali earth cations (Ca^{2+}). The number of non-bridging oxygen per tetrahedron is equal to zero assuming that the proportion of aluminium in fivefold coordination is negligible (e.g. Neuville et al. 2006). The

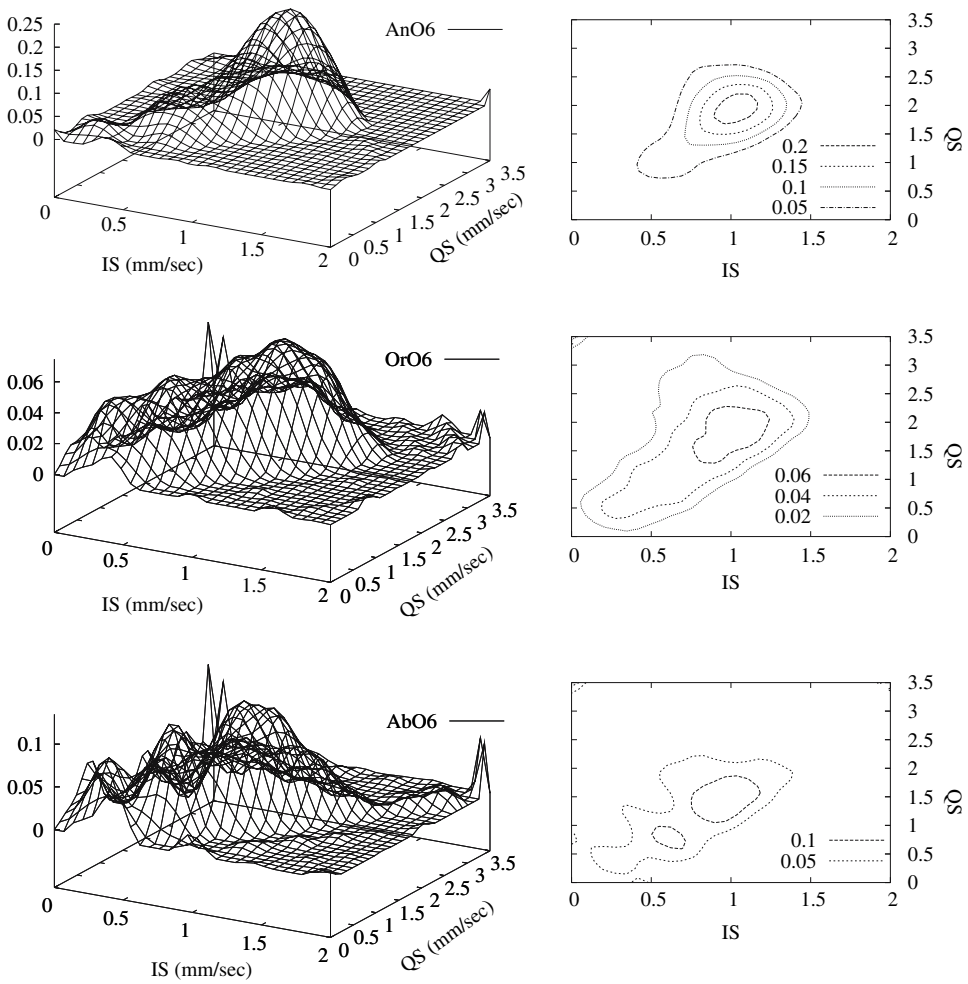

Fig. 3 Distribution of Mössbauer parameters derived from the SID method for An06, Or06 and Ab06 glasses

addition of 0.5 wt% of iron oxide in these compositions modifies the glass network by introducing a deficiency in alkalis or alkaline–earth as compared to aluminium plus iron. Because the glasses have been synthesized at the same experimental conditions the variations observed in the redox ratio show the effect of the composition on the oxidation state of iron. Additionally, the comparison between the SID distributions (3D and 2D) points out differences in the environment of iron ions in the glass. The reasons for these differences have probably to be found in the way how cations interact with anionic species and especially in the hierarchy of the strength of these interactions (Hess 1995). In particular, the competition between cations for the charge compensation of AlO_4^- unit is an important parameter.

The trend observed in the oxidation state of the samples is in good agreement with previous work. Mysen (2006) has shown that Fe^{3+}/Fe_{tot} ratio is higher for Na^+ or K^+ than for earth alkali cations in alumino-silicate glasses. Among alkalis, Na^+ is more suitable than K^+ to stabilize Fe^{3+} in good agreement with literature (Mysen and Richet 2005). In iron-alumino-silicate glasses, Antoni et al. (2004) have concluded that the substitution of Na_2O by CaO leads to a decrease of the ferric iron proportion. In peraluminous compositions, the Fe^{2+}/Fe^{3+} ratio increases as $K_2O/(K_2O + Al_2O_3 + Fe_2O_3)$ decreases reflecting that ferrous iron is required for charge compensation of AlO_4^- tetrahedron (Dickenson and Hess 1986) when potassium is lacking. This observation may suggest that K^+ is a more efficient charge compensator of the AlO_4^- unit than Fe^{2+}. In complex alumino-silicate glasses, the substitution of K_2O by CaO (everything else being equal) increases the proportion of ferrous iron in the glass (Dickenson and Hess 1986). This is in good agreement with the results observed in this study. The Ca-bearing glass is indeed the most reduced of the three samples considered. More insights into the role played by iron ions in silicate glasses cannot be derived from Mössbauer data alone but require information by other spectroscopic techniques or structural simulations.

Effect of water on iron in feldspathic glasses

A hydrated Or06 glass was used in order to investigate the effect of water on the glass structure. The Mössbauer spectra of both dry and hydrous glasses are presented in Fig. 4. The Mössbauer spectrum of the dry glass is strongly modified when water is incorporated to the silicate structure. Part of the differences observed is due to different temperature and oxygen fugacity during the synthesis, i.e. the hydrous glass was produced at lower temperature and lower oxygen fugacity, but also to quench effect. The spectrum of the hydrous glass is narrower and the asymmetry is reduced as compared to the spectrum of the dry glass.

The Mössbauer parameter distribution for the hydrous glass as obtained by the SID method is presented on Fig. 5. The distribution is strongly different from that obtained for the dry glass (Fig. 3). The ferrous iron contribution is now composed of one well defined contribution whereas in the dry glass various species were contributing to the spectrum covering the whole range of hyperfine Mössbauer parameters. In the hydrous glass, the ferric iron region is completely separated from the ferrous iron one and the ferrous iron contribution is much narrower. Due to the separation of ferrous and ferric iron contributions, the hydrous glass can be condidently fitted using the x-VBF method. The fit of the Or06hyd1 sample is presented on Fig. 4. The validity of the fit is confirmed by the similarity between the SID and x-VBF extracted distributions (Fig. 5). Two components are necessary to obtain a good fit of the experimental spectrum: one Fe^{2+} doublet and one Fe^{3+} doublet that represent, respectively, 84 and 16% of the total signal. Hyperfine Mössbauer parameters of the two contributions are given in Table 2. As compared to the apparent Mössbauer parameters of ferrous iron in the dry glass (maximum located around IS = 1 and QS = 2 mm/s), the ferrous iron IS and QS are shifted towards higher values (IS = 1.16 and QS = 2.4 mm/s) indicating a higher coordination number of ferrous iron in the hydrous glass. Due to the very low signal due to ferric iron in the dry glass, no convincing comparison of the effect of water on ferric iron coordination can be made. These results

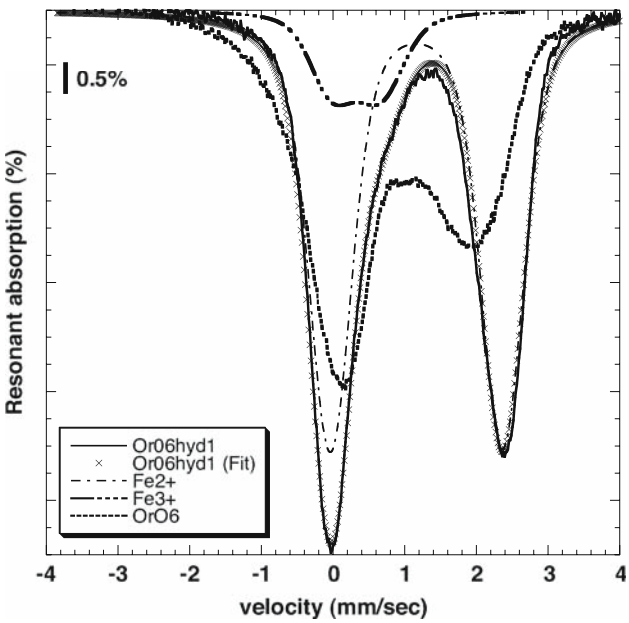

Fig. 4 Comparison of Mössbauer spectra of dry (Or06) and hydrous glass (Or06hyd1) of OrO6 composition and fit of the spectrum of the hydrous sample using the x-VBF method

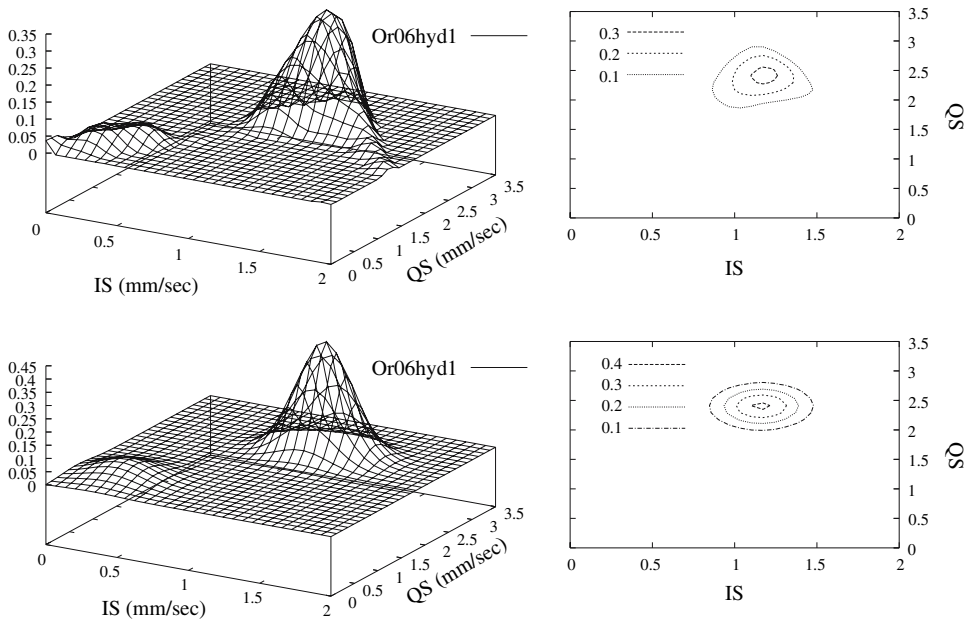

Fig. 5 Distribution of Mössbauer parameters derived from the SID (*top*) and the x-VBF (*bottom*) methods for hydrous Or06 glass. 2D plots are obtained by projecting the 3D distribution onto the (IS,QS) plane

demonstrate that the environment of iron is very sensitive to water incorporation, in good agreement with results observed for Ni^{2+} by optical absorption spectroscopy (Nowak and keppler 1998) and X-ray absorption spectroscopy (Farges et al. 2001).

Water incorporation in the silicate structure generates a sharper distribution of iron environments. A similar drastic difference between dry and hydrous glasses was observed in the second set of samples (tonalitic system) (Wilke et al. 2002). The effect of dissolved water on the structure of alumino-silicate glasses and melts is still under debate, but recent NMR studies support the hypothesis that the incorporation of water depolymerises the melt structure (Xue and Kanzaki 2006). This idea matches with observations by in situ XANES spectroscopy which indicates rapid ordering in the local environment of nickel and iron in hydrous melts near the glass transition (Farges et al. 2001; Wilke et al. 2006). These effects are not completely suppressed even when using high cooling rates and may result in formation of iron-bearing nanocrystals at slow cooling (Wilke et al. 2006). Thus the interpretation of Mössbauer spectra of glasses needs to consider both cooling rate and water content of the glasses. Although the effect of water introduction is already remarkable on the Mössbauer experimental spectrum of Or06hyd1, the analysis of the distribution shape provides important supplementary information such as the width of the hyperfine parameter distribution and the separation between ferric and ferrous iron signals as compared to classical Mössbauer data analysis. The use of these specificities will allow an improved analysis of Mössbauer spectra and may give new insights into the structure of the glasses and the ordering processes (see section on quench effects below).

Effect of redox conditions on iron in hydrous glass

The effect of oxygen fugacity has been studied on a series of hydrated glasses of haplo-tonalitic composition (Wilke et al. 2002). The raw experimental Mössbauer spectra are not reproduced in this work as they are already published (see Fig. 1 in Wilke et al. 2002). Interpretation of the Mössbauer spectra and results of fitting by SID are already given in (Wilke et al. 2002) and the findings are summarized only briefly in the following. With increasing Fe^{3+}/Fe_{tot} the shape of the Mössbauer spectra is modified and a feature peaking at 0.8 mm/s becomes more and more prominent. This feature is the high velocity branch of the signal due to ferric iron. The low velocity branch of the ferric iron signal is entirely hidden by the low velocity branch of ferrous iron signal pointing at 0 mm/s. Therefore the changes due to the variation of the oxidation state are visible but not clearly resolved. In order to better visualize the evolution of both ferrous and ferric iron signals, the 2D and 3D SID distribution of the Mössbauer parameters for Cu–Cu_2O, HM, intrinsic rapid quench, intrinsic slow quench and C–O–H hydrous samples are presented on Fig. 6 (for notation and sample characteristics see Table 2). The main advantage of this representation is that in this 2D or 3D representations the ferric iron signal is now well separated from the ferrous iron one (Fig. 6). The Fe^{3+} Mössbauer signal will appear in the bottom left part of the parallelogram while for Fe^{2+} signal will be located in the right upper part of the parallelogram.

From top to bottom, the oxygen fugacity is increasing and it is, in this representation, directly correlated to the increase of the ferric iron signal. Moreover, due to the separation of the ferrous and ferric iron signals, it is now

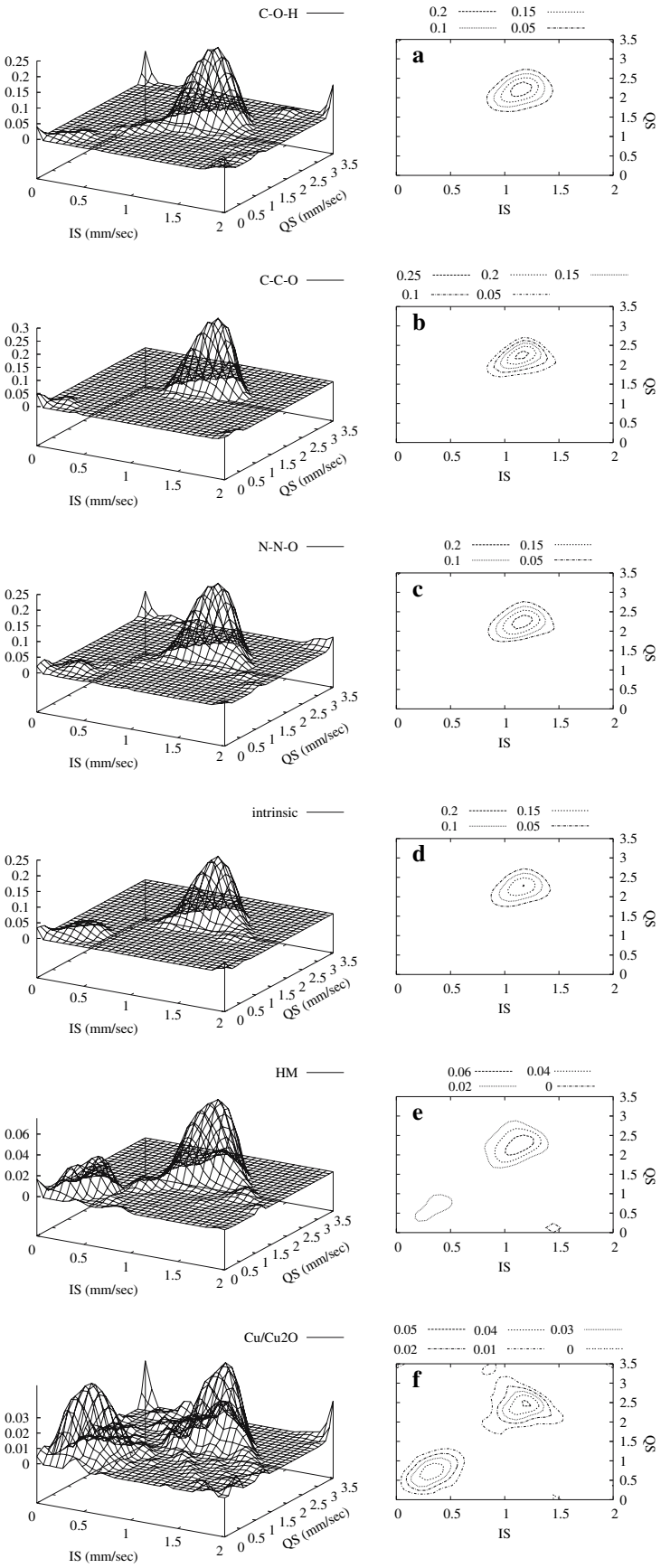

Fig. 6 Distribution of Mössbauer parameters derived from the SID method for the tonalitic series. 2D plots are obtained by projecting the 3D distribution onto the (IS,QS) plane. From top to bottom, the $Fe^{3+}/\sum$ Fe increases

Table 2 Mössbauer parameters obtained for the studied samples using the x-VBF method

Sample	Area (%)	IS	QS	ΔIS	ΔQS	θ	
Or06hyd1	84	1.16	2.40	0.18	0.23	1.55	Fe^{2+}
	16	0.33	0.67	0.18	0.31	1.55	Fe^{3+}
C–O–H 850C 500 MPa $fO_2 = -15.6$	100	1.14	2.12	0.17	0.29	18.1	Fe^{2+}
CCO 850C 500 MPa	92.4	1.14	2.18	0.15	0.24	8.1	Fe^{2+}
$fO_2 = -14.4$	7.6	0.16	0.48	0.15	0.21	8.1	Fe^{3+}
NNO 850C 500 MPa	90.9	1.14	2.18	0.16	0.28	8.1	Fe^{2+}
$fO_2 = -12.74$	9.1	0.25	0.73	0.19	0.28	8.1	Fe^{3+}
intrinsic 850C 500 MPa	88	1.15	2.24	0.14	0.29	9.8	Fe^{2+}
$fO_2 = -10.4$	12	0.34	0.64	0.11	0.12	0.00	Fe^{3+}
HM 850C 500 MPa	72.2	1.12	2.25	0.16	0.30	8.1	Fe^{2+}
$fO_2 = -8.33$	27.8	0.32	0.73	0.16	0.34	8.1	Fe^{3+}
Cu/Cu_2O 500 MPa	47.2	1.16	2.44	0.13	0.29	2.1	Fe^{2+}
$fO_2 = -7.6$	40.9	0.36	0.74	0.13	0.35	0.02	Fe^{3+}
	11.9	0.71	2.12	0.14	0.33	0.04	
Intrinsic SQ 850C							
D1	26	1.16	2.20	0.33	0.27	1.6	Fe^{2+}
D2	18	0.39	0.73	0.19	0.22	10.6	Fe^{3+}
D1′	56	1.15	2.54	0.07	0.07	2.0	Fe^{2+}
Intrinsic RQ 850C							
D1	74	1.17	2.27	0.17	0.28	8.1	Fe^{2+}
D2	26	0.36	0.78	0.17	0.22	8.1	Fe^{3+}

Area (%) is the percentage of total Mössbauer signal assigned to each contribution. IS and QS stand for the isomer shift and quadrupole splitting and are given in mm/s. IS values are given relatively to metal iron. ΔIS (resp. ΔQS) is the distribution width in the IS direction (resp. In the QS direction). θ is the correlation parameter between both directions

possible to evaluate the relative areas of the Mössbauer signal due to each species (in contrast to the dry glasses with feldspar composition). This gives directly access to the redox ratio without making any assumption on the iron speciation and its distribution in contrast to conventional Mössbauer data analysis. The Fe^{3+}/Fe_{tot} values determined by the SID method are given in Table 3. Because of small differences in the IS and QS ranges used for the determination of the oxidation state, the values are slightly different from the ones given in Wilke et al. (2002) for the same samples. Comparison with redox ratios derived from classical evaluation by Lorentzian fits can be found in Wilke et al. (2002). Although very powerful to extract the overall distribution of Mössbauer parameters, the SID method does not allow deriving accurate values of the hyperfine parameters for the various iron species (IS and QS). To go further in the structural interpretation of the Mössbauer spectra we need to decompose the experimental spectra into the ferrous and ferric iron contributions. This can be performed by using the x-VBF method. This method allows decomposing Mössbauer spectra in various Gaussian distribution of Lorentzian doublets. The fits are presented on Fig. 7. Special care was taken to avoid mathematical fits without physical significance. A criterion is the similarity of the distributions obtained by both approaches.

The 3D and 2D projections of the Mössbauer parameter distribution obtained using the x-VBF method are

Table 3 Redox ratio determined by the x-VBF and SID methods for glasses of tonalitic composition

Sample	$\frac{Fe^{3+}}{\sigma Fe}$ (x-VBF)	$\frac{Fe^{3+}}{\sigma Fe}$ (SID)	IS and QS range for redox ratio determination
C-O-H 850C 500 MPa	0	3 ± 1.6	0–0.7; 0–1.1
intrinsic 850C 500 MPa	12	12.2 ± 0.4	0–0.7; 0–1.2
Cu/Cu2O 500 MPa	40.9	39.9 ± 1.6	0–0.9; 0–1.5
CCO 850C 500 MPa	7.6	3.3 ± 0.3	0–0.7; 0–1.1
NNO 850C 500 MPa	9.1	5 ± 0.7	0–0.7; 0–1.1
HM 850C 500 MPa	27.8	21 ± 0.5	0–0.7; 0–1.1
Intrinsic SQ 850C	18	20.2 ± 0.4	0–0.5; 0–1.5
Intrinsic RQ 850C	26	24 ± 0.5	0–0.7; 0–1.7

The IS and QS parameter ranges used for the SID-redox determination are given in the last column. Errors on the SID-redox ratio have been evaluated by calculating the contribution of the region with no iron signal. It is difficult to evaluate the error bars for the x-VBF-redox ratio. It is mainly determined by the uncertainty of the fit

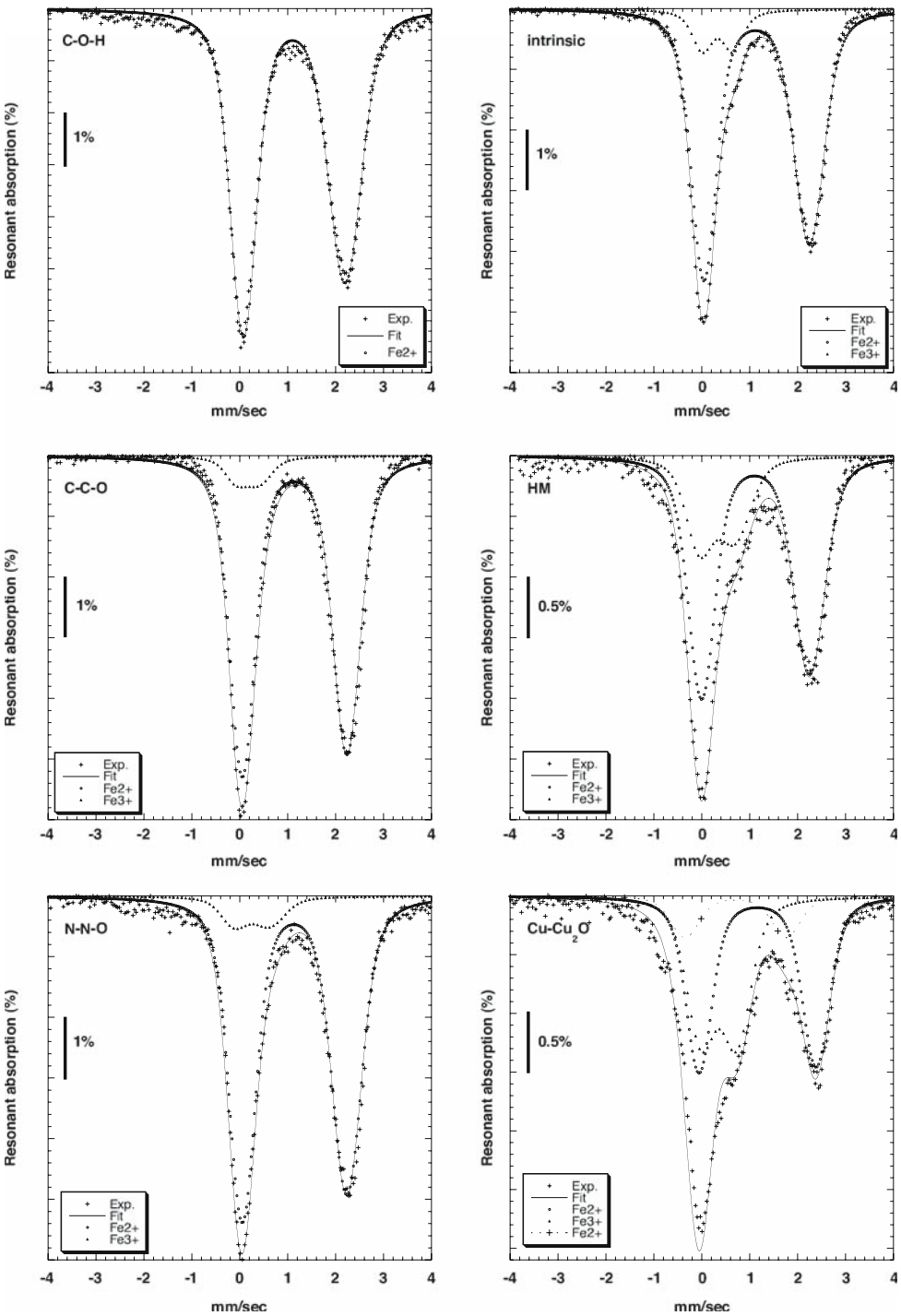

Fig. 7 Fit of the experimental spectra of the tonalitic series using the x-VBF method

presented on figure 8 and can be compared to the ones derived using the SID method (Fig. 6). Except for the most oxidized sample, the agreement between the two methods is good and validates the fits performed. The most oxidized sample is difficult to fit with the x-VBF method as the Mössbauer parameter distribution for Fe^{2+} is clearly not Gaussian as can be seen on Fig. 6f. The parameters of the fits are presented in Table 2. It has to be noted that the more reduced samples are fitted with one Fe^{2+} distribution only, whereas in fits of reduced glasses in the literature (Alberto et al. 1996; Rossano et al. 1999) two distributions were necessary in order to obtain a good agreement between experiment and fit. The difference to the samples in previous studies is the high concentration of dissolved water that narrows the distribution as was seen in the previous section for the Or06hyd1 glass. Most of the samples are thus fitted with one Fe^{2+} distribution and one Fe^{3+} distribution. The only exception is the most oxidized

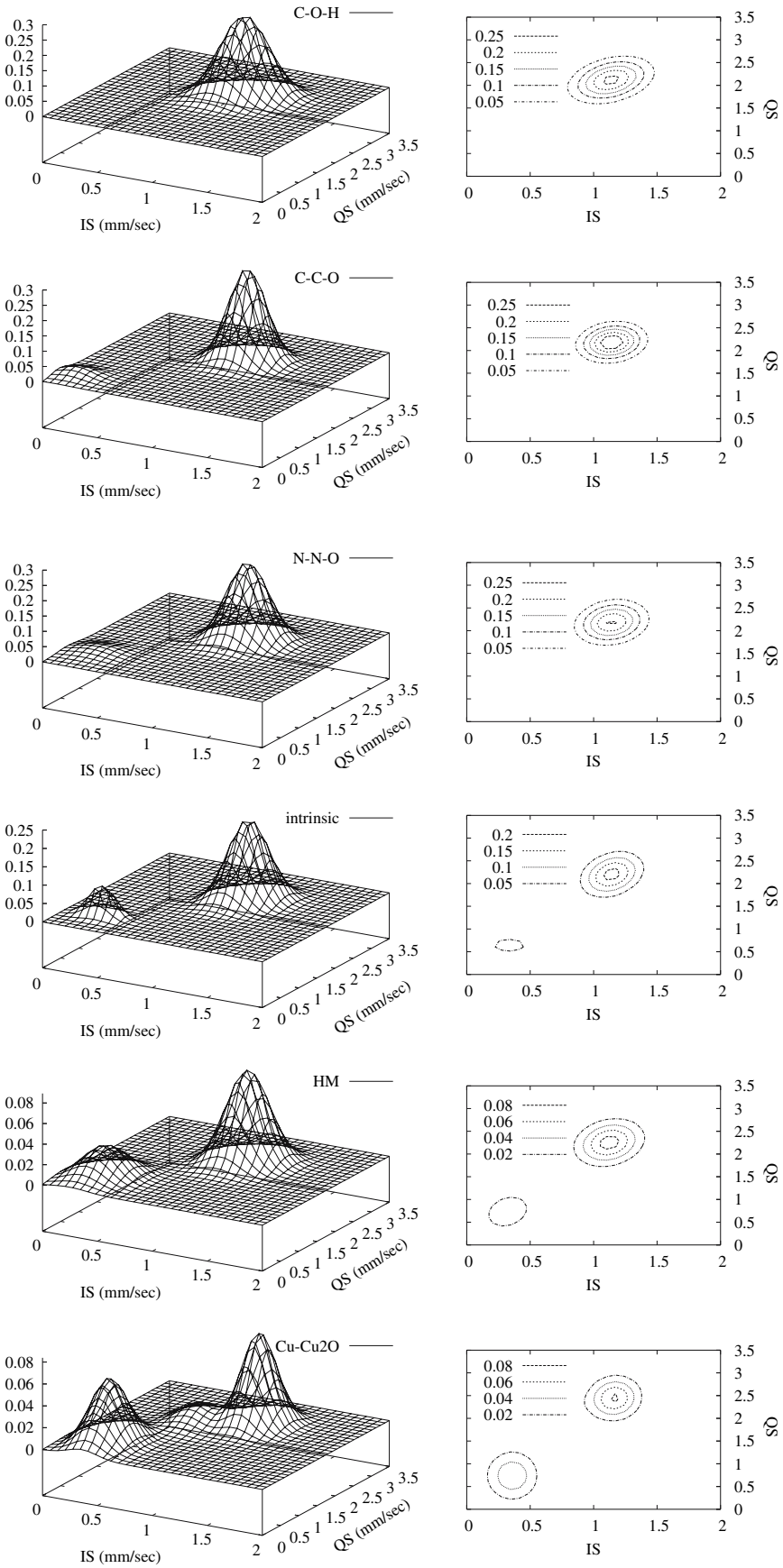

Fig. 8 Distribution of Mössbauer parameters derived from the x-VBF method. 2D plots are obtained by projecting the 3D distribution onto the (IS,QS) plane. From top to bottom, the $Fe^{3+}/\sum$ Fe increases

sample (Cu/Cu_2O) that is fitted with 3 distributions (one Fe^{3+} and two Fe^{2+}). The third contribution is necessary to compensate the non Gaussian shape of the distribution. Analysis of XANES and EXAFS spectra indicated that part of the iron is present in crystalline phases in this sample (Wilke et al. 2006), thus, providing an explanation for the presence of a third contribution.

Isomer shifts for ferrous iron extracted by the x-VBF method for the various glasses are nearly constant, i.e. do not vary with the redox ratio. In contrast the isomer shift for ferric iron increases from 0.16 mm/s to 0.36 mm/s as the redox ratio increases. The latter observation contrasts with the results obtained in previous works on dry aluminosilicate glasses (Virgo and Mysen 1985, 2006; Jayasuriya et al. 2004) where the isomer shift for ferric iron was shown to decrease as a function of Fe^{3+}/Fe_{tot}. In his 2006 work, Mysen also used the x-VBF method to analysze Mössbauer spectra. This suggests that the trend observed in the present work may be due to the incorporation of water and it is not a drawback of the analytical method used. The redox ratio evaluated by the x-VBF method is given in Table 3 and can be compared to those derived by SID and by conventional fitting. The values derived by the three methods are relatively close. However, some authors (Lange and Carmichael 1989; Ottonello 1997) pointed out that the determination of redox ratio from Mössbauer spectra by conventional fitting methods is less precise at high iron oxide content than at low iron oxide content. This may be due to the fact that at high iron oxide content, the distribution of sites is wider than at low iron oxide content and fitting by simple Lorentzian doublets becomes problematic. On the other hand, Mysen and Richet (2005) showed that ferric/ferrous ratio of glass determined by Mössbauer and wet chemical methods are in good agreement over a very wide range of total iron contents and a systematic misfit of the Mössbauer data is not evident for high iron content (their Fig. 10.4). Thus if only the redox state of iron is of interest, conventional Mössbauer fitting might be suitable for a wide range of iron contents and Fe^{2+}/Fe^{3+} ratios.

The main advantage of the two methods presented in this work is obtained in the case of highly reduced samples. In such samples, the ferric iron contribution is hidden by the low velocity branch of the ferrous iron doublet. Thus, the conventional fit of Mössbauer spectra will be difficult leading to inaccurate redox and coordination number determination due to the lack of feature to constrain the Fe^{3+} contribution parameters. The SID method used in this work does not have the same drawbacks. If the ferric and ferrous iron signals are well separated on the distribution plot, the redox ratio can be determined regardless of the relative abundance of the two species. However, we should keep in mind that some glasses show a continuous distribution even between the Fe^{3+} and Fe^{2+} regions. This is found for synthetic glasses (such as the ones presented in the previous section) but also for highly reduced natural glasses containing a small amount of water such as Median Ocean Ridge Basalts (MORB) of the Atlantic ocean (Fig. 9). In this case, the redox ratios derived by both conventional and more advanced methods might be dependent of the fit model. Concerning the IS and QS determination, the validation of the x-VBF fit by comparing the x-VBF distribution to the SID one ensures the physical meaning of the fit and thus of the parameters obtained.

Quench effects

In previous work Wilke et al. (2002) the effect of the quench rate on iron ions distribution was qualitatively studied by comparing the Mössbauer spectrum of two samples of the haplo-tonalitic series : the slowly quenched sample (SQ) and the rapid quenched sample (RQ). The experimental spectrum of the slowly quenched (SQ) sample (150 K/min above 500°C; 100 K/min between 500 and 360°C; 1 K/min down to room temperature) is narrower than the rapidly quenched (RQ) one (>150 K/s), at least for a part of the signal.

In order to get more information on the iron speciation in these two samples, the experimental spectra were decomposed in this study using the x-VBF method. Two contributions were sufficient to model the RQ sample spectrum while three contributions were necessary to fit the SQ sample spectrum (Fig. 10). The refined parameters are given in Table 2. To ensure the validity of the fits, the distributions obtained using the x-VBF method were compared to the ones obtained by the SID method (Figs. 11, 12 for the RQ and SQ samples, respectively). The similarity is good for the RQ sample justifying the Gaussian shape approximation of the distribution. However a good fit of the SQ spectrum is difficult to obtain due to

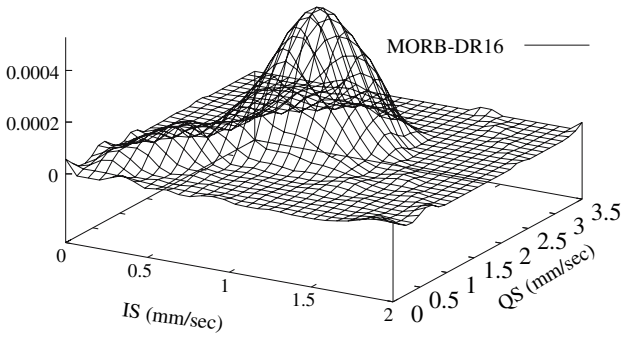

Fig. 9 SID distribution of Mössbauer parameters for a natural basaltic glass of mid-ocean ridge (Bézos and Humler 2005)

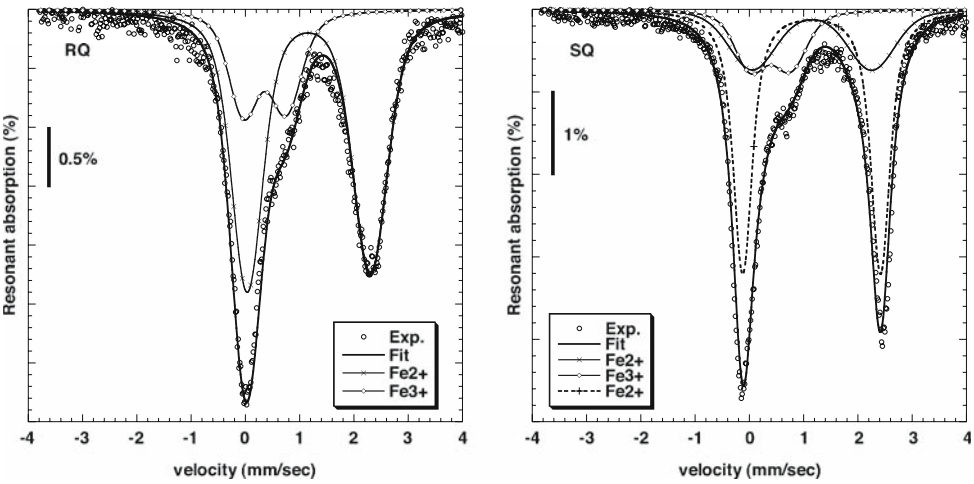

Fig. 10 Fits of the experimental spectra of the slowly quenched and rapidly quenched samples realised with the x-VBF method

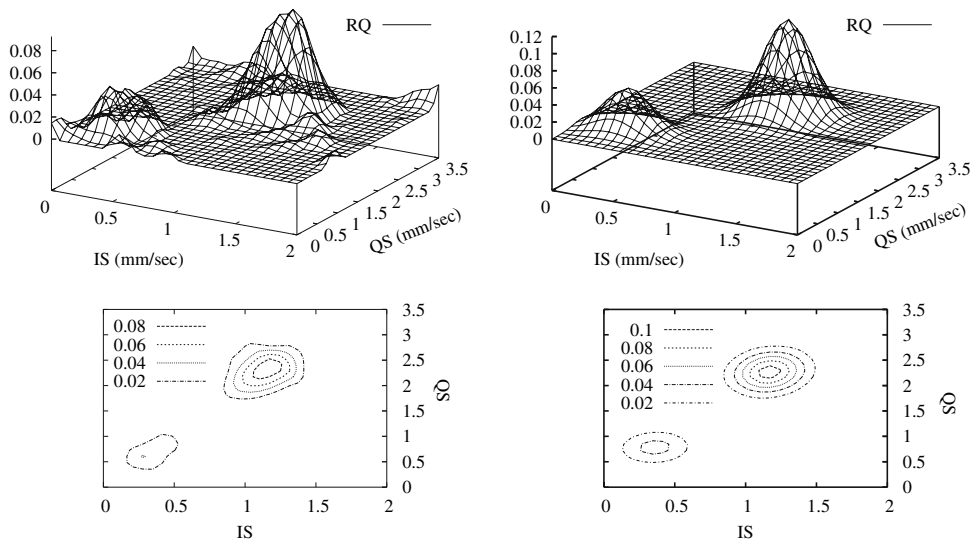

Fig. 11 SID (*left*) and x-VBF (*right*) 2D and 3D distribution plots for the rapid quenched sample

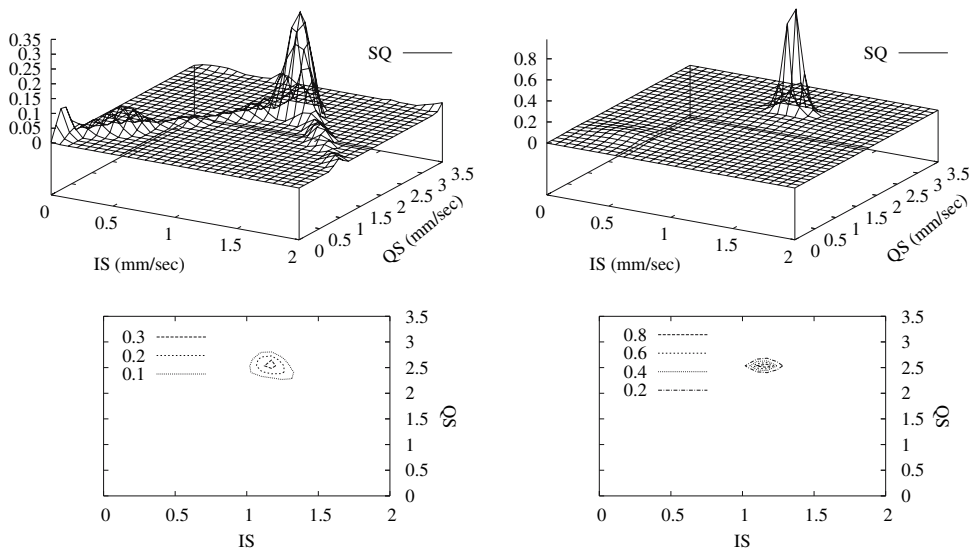

Fig. 12 SID (*left*) and x-VBF (*right*) 2D and 3D distribution plots for the slow quenched sample

the non Gaussian shape of the distribution (Fig. 12). The two distributions used to fit the RQ sample spectrum are described by two sets of IS and QS values: D1:IS = 1.17 mm/s; QS = 2.27 mm/s and D2:IS = 0.36 mm/s; QS = 0.78 mm/s. These sets of values are typical for Fe^{2+} in an octahedral site and Fe^{3+} in a five or sixfold coordinated site based on a comparison with iron hyperfine parameters in crystalline compounds (Burns 1994). In the SQ sample fit, these two distributions are still present (with slightly different parameters) but a supplementary contribution (D1') has to be introduced. This third contribution can be attributed to Fe^{2+} in an octahedral site of slightly different distortion than D1 (D1':IS = 1.15 mm/s; QS = 2.53 mm/s). This contribution is much narrower than the D1 doublet ($\Delta IS = \Delta QS = 0.07$ mm/s instead of $\Delta IS = 0.33$; $\Delta QS = 0.27$ mm/s). D1' is thus attributed to an ordered environment. The proportion of ferrous iron in the glass phase and in the ordered environment accounts to 32 % and 68 %, respectively. It has to be noted that D1 is also slightly narrower in the SQ sample ($\Delta IS = 0.17$ mm/s) as compared to the RQ sample ($\Delta IS = 0.33$ mm/s). This is in good agreement with the assumption that the vitreous phase becomes depleted in iron in the SQ sample. It is unlikely that Fe^{2+} only enters the crystalline phase. Based on TEM observation of the SQ sample (Wilke et al. 2006) have proposed the presence of either Fe_2O_3 or Fe_3O_4 as crystalline phase in that sample. Moreover, iron-rich nanocrystals were observed in hydrous andesitic glasses after annealing near the glass transition and ferric iron was shown to promote the exsolution of iron oxides in supercooled melts (Liebske et al. 2003). However a narrow contribution for Fe^{3+} does not clearly appear on the experimental Mössbauer spectrum of the SQ sample as it is most probably hidden by the ferrous iron contribution. The occurrence of both vitreous and crystalline phases in various proportions in the SQ and RQ samples is in good agreement with EXAFS results and transmission electron microscopy observations, which have shown that a major part of the iron is in nanocrystals (Wilke et al. 2006). The Fe K-edge XANES and EXAFS spectra of the SQ sample have been shown to be much more structured than the RQ sample ones (Wilke et al. 2006) indicating a more ordered environment around iron in that sample. The XANES/EXAFS spectra of the SQ sample indicate particularly contribution by Fe-Fe pairs similar to those found in Fe_2O_3 or Fe_3O_4. However, X-ray absorption spectroscopy records an average signal for all iron ions in any environment. On the other hand, the deconvolution of Mössbauer spectra by the advanced analytical methods proposed here allows not only separating signals arising from ferric and ferrous iron but also from crystallised and amorphous components. In the latter case, the different contributions are characterized by their average hyperfine parameters (IS and QS) but also by the widths of the distributions. This ability to extract precise information on various components might provide an important help to understand and quantify the crystallization kinetics in glasses near the glass transition. Combination of Mössbauer spectroscopy with experimental series in which the cooling rate and/or isothermal annealing duration is varied in the temperature range of the glass transition may provide insights into the mechanisms of exsolution of iron oxides from glasses.

Iron coordination in glasses

The results presented in this work do confirm our views on ferrous iron speciation in anhydrous glasses. Whatever the composition (feldspar or tonalitic) ferrous iron is present in a wide distribution of sites mainly centred on fivefold coordinated Fe^{2+} with small amount of four and sixfold coordinated Fe^{2+} (based on the qualitative observation of the distributions). The occurrence of this special coordination (5-fold) is now well documented by various techniques: XAS (Rossano et al. 2000a; Wilke et al. 2007), Optical absorption spectroscopy (Lefrère 2002), Mössbauer (Rossano et al. 1999), Optical magnetic circular dichroism (Jackson et al. 2005). In the case of the hydrous samples, ferrous iron does behave in a different manner. We have shown that in these quenched samples, ferrous iron is mainly located in 6-fold coordinated sites in good agreement with results obtained by Fe K-pre-edge analysis (Wilke et al. 2006). It has to be noted that the effect of composition does not seem to be as critical as expected. Indeed, the Mössbauer parameters obtained for the Or06hyd1 sample and for the HM sample, which present a similar redox ratio, are very close to each other (Table 2). This behaviour of ferrous iron in quenched glasses is most probably associated to quench effect. Analysis of spectra taken on hydrous haplogranitic melt in-situ at high temperature and pressure provides strong evidence that the local structural environment of ferrous iron is not affected by the H_2O dissolved in the melt (Wilke et al. 2006). These assumptions have however to be confirmed by further investigation.

Ferric iron coordination in glasses is discussed more controversially. First EXAFS measurements of ferric iron environment have concluded that Fe^{3+} was in a tetrahedral site (Calas and Petiau 1983). Furthermore, due to similarity in charge and ionic radius between Fe^{3+} and Al^{3+}, ferric iron in glasses has been considered as a network former located in a tetrahedral site. However, systematic comparison between ferrisilicate and alumino-silicate properties show differences between the two systems suggesting that Fe^{3+} is probably not as similar to Al^{3+} in the glass structure as is usually considered (Mysen and Richet 2005). Recent X-ray

absorption measurements combined with Molecular Dynamics simulation have proposed higher coordination for ferric iron (Farges et al. 2004; Wilke et al. 2005, 2007). In this work, the Mössbauer parameters obtained for ferric iron in different glass compositions (anhydrous and quenched hydrous samples) do vary strongly. In anhydrous glasses with feldspar composition, the ferric iron distribution is very wide suggesting no preferential location. By contrast, the optical absorption spectrum of Ab06 is rather similar to feldspars in the range of Fe^{3+} bands and Fe^{3+} is generally assigned to tetrahedral sites in these minerals. However considering the very small intensity of the Fe^{3+} bands, it is very likely that five or sixfold coordinated ferric iron does not give any detectable signal in optical absorption spectroscopy. In the haplo-tonalitic series, IS varies between 0.16 and 0.36 mm/s while QS varies from 0.48 to 0.76 mm/s in the Fe^{3+} region. This suggests that ferric iron can occupy of course tetrahedral site (in very reduced sample such as CCO). However as soon as the glass becomes more oxidized, the IS of ferric iron increases suggesting that ferric iron starts to enter sites with higher coordination such as five and sixfold coordinated site. The occurrence of fivefold coordinated site for ferric iron cannot be dismissed as ferric iron parameters in Cu/Cu_2O buffered sample (IS = 0.36 mm/s; QS = 0.74 mm/s) are very close to the ones of yoderite crystal (Dyar et al. 1991), that contains fivefold coordinated Fe^{3+} (Abu-Eid et al. 1978). Of course, the data presented here do not cover a large enough basis in terms of composition to present a complete view on the speciation of iron in oxide glasses. The major idea that should be retained is that the analytical procedures and examples presented here clearly show that both, ferric and ferrous iron, are present in a wide and continuous distribution of environment in glasses.

Conclusion

Spectroscopic studies on glasses are often difficult to interpret due to the lack of long-range order and to the wide distribution of sites available. An improved analytical procedure for evaluation of Mössbauer spectra adapted to disordered systems provides information on iron site geometry but also on the distribution of iron environments and thus on the structural disorder associated to iron. In particular, the possibility to extract the probability distribution of Mössbauer hyperfine parameters offers new insights into the structural environment of iron. The shape and the extent of the distribution provide qualitative information on the structural disorder/dispersion of ferrous and ferric iron in the glass. The advanced analysis with the SID method allows identifying continuous distributions covering the range from ferric iron to ferrous iron regions. Even the x-VBF method does not offer this possibility because of the imposed Gaussian shape of the distribution. As a consequence, it has to be noted that the IS variation in glasses may be important implying that analytical methods based on QS distribution only are not always sufficient to reproduce glass spectra. Besides, the comparison of the SID and x-VBF distributions is fundamental to validate the fit of the experimental spectrum and helps avoiding numerical fits without physical meaning. Once validated the fit performed using the x-VBF method provides information on the various iron species contributing to Mössbauer spectra.

In favourable cases, the ferrous and ferric iron contributions to the experimental spectrum are separate on the SID probability distribution plot. This is an important feature as it allows discriminating between ferrous and ferric iron signal in contrast to X-ray absorption spectroscopy (for example) that gives access to an average signal, only. The separation of ferrous and ferric iron contributions allows a precise determination of the redox ratio without making any assumption on iron environment—which is a serious limitation of conventional Mössbauer spectra analysis. Further refinement of redox ratio determination needs to take into account the difference in recoil free fraction for ferrous and ferric iron ions. Up to now, Fe^{3+} and Fe^{2+} recoil free fractions are considered to be equal in silicate glasses. This is most certainly not correct as some works have pointed out differences between redox ratio determined at room temperature and at low temperatures (Nishida 1995; Mysen 2006). New measurements of the recoil free fractions of iron ions are in progress for basaltic glasses. These are however difficult to perform considering the wide distribution of sites that will present different recoil free fractions. Finally the possibility to extract a part of the Mössbauer signal only may be very usefull to analyse complex systems composed of various Fe-bearing phases as it is most of the time the case in natural systems.

Acknowledgments The authors thank A. Bezos who kindly provided the natural MORB Mössbauer spectrum. Furthermore we would like to thank S. Hafner and D. Burkhard for assistance in collection of Mössbauer spectra at the university of Marburg. Special thanks to F. Farges who provides the authors with a review of this manuscript and to T. Berkover for his mathematical help. Authors thank B. Mysen and an anonymous reviewer for their constructive remarks.

References

Abu-Eid RM, Langer K, Seifert F (1978) Optical absorption and Mössbauer spectra of purple and green yoderite, a kyanite-related mineral. Phys Chem Minerals 3:271–289

Alberto HV, da Cunha JLP, Mysen BO, Gil JM, de Campos Ayres N (1996) Analysis of Mössbauer spectra of silicate glasses using a

two dimensional Gaussian distribution of hyperfine parameters. J Non-Crystalline Solids 194:48–57

Amthauer G, Grodzicki M, Lottermoser W, Redhammer G (2004) Mössbauer spectroscopy: basic principles. In: Beran A, Libowitzky E (eds) Spectroscopic methods in mineralogy, vol 6 of EMU notes in mineralogy, Chap 8. Eötvös University Press, Budapest, pp 345–367

Antoni A, Montagne L, Daviero S, Palavit G, Bernard J-L, Wattiaux A, Vezin H (2004) Structural characterization of iron-aluminosilicate glasses. J Non-Crystalline Solids 345–346:66–69

Balan E, Allard T, Boizot B, Morin G, Muller J-P (1999) Structural Fe^{3+} in natural kaolinites: new insights from electron paramagnetic resonance spectra fitting at X and Q-band frequencies. Clays Clay Minerals 47(5):605–616

Berndt J, Liebske C, Holtz F, Freise M, Nowak M, Ziegenbein D, Hurkuck W, Koepke J (2002) A combined rapid-quench and H_2-membrane setup for internally heated pressure vessels: Description and application for water solubility in basaltic melts. Am Mineral 87:1717–1726

Berry AJ, O'Neill HS, Jayasuriya KD, Campbell SJ, Foran GJ (2003) XANES calibrations for the oxidation state of iron in a silicate glass. Am Mineral 88(7):967–977

Bézos A, Humler E (2005) The $Fe^{3+}/\sum$ Fe ratios of MORB glasses and their implications for mantle melting. Geochim Cosmochim Acta 69(3):711–725

Boizot B, Ollier N, Olivier F, Petite G, Ghaleb D, Malchukova E (2005) Irradiation effects in simplified nuclear waste glasses. Nucl Instrum Methods Phys Res B 240:146–151

Bonnin-Mosbah M, Simionovici AS, Metrich N, Duraud JP, Massare D, Dillmann P (2001) Iron oxidation states in silicate glass fragments and glass inclusions with a XANES micro-probe. J Non-Crystalline Solids 288:103–113

Bonnin-Mosbah M, Metrich N, Susini J, Salomé M, Massare D, Menez B (2002) Micro X-ray absorption near edge structure at the sulfur and iron K-edges in natural silicate glasses. Spectrochim Acta B 57:711–725

Botcharnikov RE, Koepke J, Holtz F, McCammon C, Wilke M (2005) The effect of water activity on the oxidation and structural state of Fe in a ferro-basaltic melt. Geochim Cosmochim Acta 69(21):5071–5085

Burns RG (1994) Mineral Mössbauer spectroscopy:correlations between chemical shift and quadrupole splitting parameters. Hyperfine Interact 91:739–745

Calas G, Petiau J (1983) Coordination state of iron in oxide glasses through high resolution K-edge spectra: information from pre-edge. Solid state Commun 48:625–629

Dickenson MP, Hess PC (1986) The structural role and homogeneous redox equilibria of iron in peraluminous, metaluminous and peralkaline silicate melts. Contrib Mineral Petrol 92:207–217

Dunlap RA (1997) An investigation of Fe oxidation states and site distributions in a tibetan tektite. Hyperfine Interact 110:217–225

Dyar MD, Perry CL, Rebbert CR, Dutrow BL, Holdaway MJ, Lang HM (1991) Mössbauer spectroscopy of synthetic and naturally occurring staurolite. Am Mineral 76(1–2):27–41

Ehrt D, Leister M, Matthai A (2001) Polyvalent elements iron, tin and titanium in silicate, phosphate and fluoride glasses and melts. Phys Chem Glasses 42(3):231–239

Evans RJ, Rancourt DG, Grodzicki M (2005) Hyperfine electric field gradients and local distortion environments of octahedrally coordinated Fe^{3+}. Am Mineral 90:187–198

Farges F, Munoz M, Siewert R, Malavergne V, Brown GE, Behrens H, Nowak M, Petit P-E (2001) Transition elements in water-bearing silicate glasses/melts. Part II. Ni in water-bearing glasses. Geochim Cosmochim Acta 65(10):1679–1693

Farges F, Lefrère Y, Rossano S, Berthereau A, Calas G, Brown GE (2004) The effect of redox state on the local structural environment of iron in silicate glasses: a molecular dynamics, combined XAFS spectroscopy, bond valence study. J Non-Crystalline Solids 344(3):176–188

Galoisy L, Calas G, Arrio M-A (2001) High-resolution XANES spectra of iron in minerals and glasses: structural information from the pre-edge region. Chem Geol 174(1–3):307–319

Giuli G, Paris E, Pratesi G, Koeberl C, Cipriani C (2003) Iron oxidation state in the Fe-rich layer and silica matrix of Libyan Desert Glass: a high-resolution XANES study. Meteorit Planet Sci 38(8):1181–1186

Giuli G, Eeckhout SG, Paris E, Koeberl C, Pratesi G (2005) Iron oxidation state in impact glass from the K/T boundary at Beloc, Haiti, by high-resolution XANES spectroscopy. Meteorit Planet Sci 40(11):1575–1580

Gunnlaugsson HP (2006) A simple model to extract hyperfine interaction distributions from Mössbauer spectra. Hyperfine Interact 167:851–854

Hannoyer B, Lenglet M, Dürr J, Cortes R (1992) Spectroscopic evidence of octahedral iron (III) in soda-lime silicate glasses. J Non-Crystalline Solids 151:209–216

Hess PC (1995) Thermodynamic mixing properties and the structure of silicate melts. In: Stebbins JF, Millan PFM, Dingwell DB (eds) Structure, dynamics and properties of silicate melts, vol 32 of Reviews in Mineralogy. Mineralogical Society of America, pp 145–189

Hofmeister A, Rossman GR (1984) Determination of Fe^{3+} and Fe^{2+} concentrations in feldspar by optical absorption and EPR spectroscopy. Phys Chem Minerals 11:213–224

Jackson WE, Farges F, Yeager M, Mabrouk PA, Rossano S, Waychunas GA, Solomon EI, Brown GE (2005) Multi-spectroscopic study of Fe(II) in silicate glasses: implications for the coordination environment of Fe(II) in silicate melts. Geochim Cosmochim Acta 69:4315–4332

Jayasuriya KD, O'Neill HS, Berry AJ, Campbell AJ (2004) A Mössbauer study of the oxidation state of Fe in silicate melts. Am Mineral 89:1597–1609

Karabulut M, Marasinghe GK, Ray CS, Ray DE, Waddill GD, Booth CH, Allen PG, Bucher JJ, Caulder DL, Shuh DK (2002) An investigation of the local iron environment in iron phosphate glasses having different Fe(II) concentrations. J Non-Crystalline Solids 306:182–192

Lagarec K, Rancourt DG (1997) Extended Voigt-based analytic lineshape method for determining N-dimensional correlated hyperfine parameter distributions in Mössbauer spectroscopy. Nucl Instrum Methods Phys Res B 129:266–280

Lange RA, Carmichael ISE (1989) Ferric-ferrous equilibria in Na_2O–FeO–Fe_2O_3–SiO_2 melts: effects of analytical techniques on derived partial molar volumes. Geochim Cosmochim Acta 53:2195–2204

Lefrère Y (2002) Propriétés d'absorption optique du Fe^{2+} et du Fe^{3+} dans des verres d'intérêt industriel: mesure, modélisation et implications structurales. PhD Thesis, Université Denis Diderot

Leister M, Ehrt D (1999) Redox behavior of iron and vanadium ions in silicate melts at temperature up to 2000°c. Glass Sci Technol 72(5):153–160

Levitz P, Bonnin D, Calas G, Legrand A-P (1980) A two-parameter distribution analysis of Mössbauer spectra in non-crystalline solids using general inversion method. J Phys E Sci Instrum 13:427–432

Liebske C, Behrens H, Holtz F, Lange RA (2003) The influence of pressure and composition on the viscosity of andesitic melts. Geochim Cosmochim Acta 67:473–485

Magnien V, Neuville DR, Cormier L, Roux J, Hazemann JL, Pinet O, Richet P (2006) Kinetics of iron redox reactions in silicate liquids: a high-temperature x-ray absorption and Raman spectroscopy study. J Nucl Mater 352(1–3):190–195

Mc Cammon CA (2004) Mössbauer spectroscopy: applications. In: Beran A, Libowitzky E (eds) Spectroscopic methods in mineralogy, Vol 6 of EMU notes in Mineralogy, Chap 9. Eötvös University Press, Budapest, pp 369–398

Metrich N, Susini J, Foy E, Farges F, Massare D, Sylla L, Lequien S, Bonnin-Mosbah M (2006) Redox state of iron in peralkaline rhyolitic glass/melt: X-ray absorption micro-spectroscopy experiments at high temperature. Chem Geol 231(4):350–363

Mosbah M, Duraud JP, Metrich N, Wu Z, Delaney JS, San Miguel A (1999) Micro-XANES with synchrotron radiation: a complementary tool of micro-PIXE and micro-SXRF for the determination of oxidation state of elements. Application to geological materials. Nucl Instrum Methods Phys Res B 158(1–4):214–220

Mysen BO (2006) The structural behavior of ferric and ferrous iron in aluminosilicate glass near meta-aluminosilicate joins. Geochim Cosmochim Acta 70(9):2337–2353

Mysen BO, Richet P (2005) Silicate glasses and melts, vol 10 of developments in geochemistry. Elsevier, Amsredam

Nemtsova OM (2006) The method of extraction of subspectra with appreciably different values of hyperfine interaction parameters from Mössbauer spectra. Nucl Instrum Methods Phys Res B 244:501–507

Neuville DR, Cormier L, Massiot D (2006) Al coordination and speciation in calcium aluminosilicate glasses: effects of composition determined by Al-27 MQ-MAS NMR and Raman spectroscopy. Chem Geol 229(1–3):173–185

Nishida T (1995) Mössbauer effect in inorganic glasses. Hyperfine Interact 95:23–39

Nowak M, keppler H (1998) The influence of water on the environment of transition metals in silicate glasses. Am Mineral 83(1–2):43–50

Ottonello G (1997) Principles of geochemistry. Columbia university press, Columbia

Partzsch GM, Lattard D, McCammon C (2004) Mössbauer spectroscopic determination of Fe^{3+}/Fe^{2+} in synthetic basaltic glass: a test of empirical f_{O_2} equations under superliquidus and subliquidus conditions. Contrib Mineral Petrol 147:565–580

Quartieri S, Riccardi MP, Messiga B, Boscherini F (2005) The ancient glass production of the Medieval Val Gargassa glasshouse: Fe and Mn XANES study. J Non-Crystalline Solids 351(37–39):3013–3022

Rancourt DG, McDonald AM, Lalonde AE, Ping JY (1993) Mössbauer absorber thickness for accurate site populations in Fe-bearing minerals. Am Mineral 78:1–7

Rancourt DG, Christie IAD, Royer M, Kodama H, Robert J-L, Lalonde AE, Murad E (1994a) Determination of accurate $^{[4]}Fe^{3+}$, $^{[6]}Fe^{3+}$ and $^{[6]}Fe^{2+}$ site populations in synthetic annite by mössbauer spectroscopy. Am Mineral 79:51–62

Rancourt DG, Ping JY, Berman RG (1994b) Mössbauer spectroscopy of minerals. Phys Chem Minerals 21:258–267

Rancourt DG, Ping JY, Boukili B, Robert J-L (1996) Octahedral-site Fe^{2+} quadrupole splitting distributions from Mössbauer spectroscopy along the (OH, F)-annite join. Phys Chem Minerals 23:63–71

Rossano S, Balan E, Morin G, Bauer J-P, Calas G, Brouder C (1999) ^{57}Fe Mössbauer spectroscopy of tektites. Phys Chem Minerals 26:530–538

Rossano S, Ramos A, Delaye J-M, Creux S, Filipponi A, Brouder C, Calas G (2000a) EXAFS and molecular dynamics combined study of $CaO–FeO–2SiO_2$ glass. New insight into site significance in silicate glasses. Europhysics Letters 49(5):597–602

Rossano S, Ramos AY, Delaye J-M (2000b) Environment of ferrous iron in $CaFeSi_2O_6$ glass: contributions of EXAFS and molecular dynamics. J Non-Crystalline Solids 273(1–3):48–52

Stolper E (1982) Water in silicate glasses-an infrared spectroscopic study. Contrib Mineral Petrol 81(1):1–17

Uchino T, Nakaguchi K, Nagashima Y, Kondo T (2000) Prediction of optical properties of commercial soda-lime-silicate glasses containing iron. J Non-Crystalline Solids 261:72

Virgo D, Mysen B (1985) The structural state of iron in oxidized vs. reduced glasses at 1 atm: a ^{57}Fe Mössbauer study. Phys Chem Minerals 12:65–76

Wilke M, Farges F, Petit P-E, Brown GE, Martin F (2001) Oxidation state and coordination of Fe in minerals: an Fe K-XANES spectroscopic study. Am Mineral 86(5–6):714–730

Wilke M, Behrens H, Burkhard DJM, Rossano S (2002) The oxidation state of iron in silicic melt at 500 MPa water pressure. Chem Geol 189:55–67

Wilke M, Partzsch GM, Bernhardt R, Lattard D (2005) Determination of the iron oxidation state in basaltic glasses using XANES at the Fe K-edge. Chem Geol 220(1–2):141

Wilke M, Schmidt C, Farges F, Malavergne V, Gautron L, Simionovici A, Hahn M, Petit P-E (2006) Structural environment of iron in hydrous aluminosilicate glass and melt-evidence from X-ray absorption spectroscopy. Chem Geol 229:144–161

Wilke M, Farges F, Partzsch GM, Schmidt C, Behrens H (2007) Speciation of Fe in silicate glasses and melts by in-situ XANES spectroscopy. Am Mineral 92:44–56

Xue X, Kanzaki M (2006) Depolymerization effect of water in aluminosilicate glasses: direct evidence from $^{1}H–^{27}Al$ heteronuclear correlation NMR. Am Mineral 91:1922–1926